A variety of new tri- and tetranuclear Mn–Ln and Fe–Ln (Ln = lanthanide) complexes

Shreya Mukherjee, Matthew R. Daniels, Rashmi Bagai, Khalil A. Abboud, George Christou, Christos Lampropoulos *

Department of Chemistry, University of Florida, Gainesville, FL 32611-7200, USA

ARTICLE INFO

ABSTRACT

The use of carboxylates in the synthesis of 3d/4f clusters, with or without a second organic ligand, has afforded a series of tetranuclear M_2Gd_2 complexes (M = Fe or Mn), and two new trinuclear M_2Gd (M = Fe or Mn) molecular compounds. Only one of these, $[Mn_2Gd_2O_2(O_2CBu^t)_8(HO_2CBu^t)_4]$ (**1**), does not contain a multidentate chelate ligand. Two other similar tetranuclear clusters were synthesized from the use of triethanolamine ($teaH_3$) and 1,1,1-tris(hydroxymethyl)ethane ($thmeH_3$). $[Mn_2Gd_2(O-H)_2(O_2CPh)_4(NO_3)_2(teaH)_2]$ (**2**) has very similar structure with **1**, bearing a defective incomplete double-cubane core bridged by μ_3-O atoms, whereas in the core of $[NHEt_3]_2[Fe_2Gd_2(O_2CPh)_4(thme)_2(NO_3)_4]$ (**3**) the $thme^{3-}$ ligand caps the two incomplete cubane units, providing the triply-bridging alkoxides needed for bridging. Two new oxide-centered triangular clusters were synthesized bearing the Schiff-based chelate 2-{[2-(dimethylamino)ethyl]methylamino}ethanol (dmemH), namely $[Fe_2GdO(O_2C-Bu^t)_2(dmem)_2(NO_3)_3]$ (**4**), and $[Mn_2GdO(O_2CBu^t)_2(dmem)_2(NO_3)_3]$ (**5**). Magnetic susceptibility measurements and/or reduced magnetization studies established that complexes **1** and **3** have an $S = 5$ ground state, complex **2** has $S = 4$, and complexes **4** and **5** are $S = 7/2$ in their ground states. These complexes portray the feasibility of obtaining products bearing metal cores commonly found in homometallic clusters, even when these include metals with completely different coordination chemistry and electronic structure, such as lanthanides.

© 2009 Elsevier Ltd. All rights reserved.

1. Introduction

Mixed-metal materials have been attractive to solid-state chemists and condensed-matter physicists for many years as routes to new metal alloys, intermetallics, and perovskite-type metal architectures [1]. The importance of these materials arises from their heterometallic nature, which together with other factors can result in properties such as ferromagnetism, ferroelectricity, ferroelasticity and ferrotoroidicity [2]. Molecular chemists have been also interested in mixed-metal complexes for a variety of reasons. For example, heterometallic complexes are known in biology as the active sites of many enzymes, such as nitrogenase [3], mammalian superoxide dismutase [4], phosphatases [5], the water oxidizing complex near Photosystem II [6], and others [7]. Polynuclear 3d/4f complexes have also been investigated in the field of molecule-based magnets and single-molecule magnets (SMMs) as an alternative to homometallic transition metal compounds [8]. SMMs are individual molecules that can function as nanoscale magnetic particles below a blocking temperature; this property is intrinsic to the molecule and is not due to intermolecular interactions as in traditional magnets or molecule-based magnets [9].

With the main requirements for SMMs being a high spin ground state and a large uniaxial anisotropy [10], 3d/4f clusters are a logical extension to homometallic SMMs because of the large single-ion anisotropy most trivalent lanthanides possess, and to date several 3d/4f species have been identified as SMMs [11]. In order to achieve a deeper understanding of the magnetic properties of such molecules, it is useful to consider small 3d/4f clusters that would allow an investigation of the transition metal–lanthanide exchange interactions [12], and this is one of the objectives of the present work. The unpaired electrons of a lanthanide reside in 4f orbitals, which leads to weak exchange coupling, and the rare earth ion thus behaves as a free ion to a first approximation [13]. Also, the spin–orbit coupling is much larger for a trivalent lanthanide than for a 3d metal ion, which further complicates the magnetic investigation of heterometallic complexes. In this respect, isotropic lanthanides are useful in order to probe the magnetic properties of 3d/4f clusters [11e,12b].

Several synthetic strategies have been employed by molecular chemists in the search for new structural types of 3d/4f complexes and interesting magnetic properties. One such strategy is the employment of small flexible ligands such as carboxylates (O_2CR^-). Carboxylates are versatile ligand types, since the R group can vary from simple alkyl to bulkier phenyl moieties, and even functionalized R groups facilitating specific properties or behavior

---

(electrochemical, spectroscopic, surface-binding ability, etc.) [10a,14]. Dicarboxylates have also been used, albeit not extensively [15]. Other ligands that have been central players in the formation of polynuclear clusters have been the extended families of oximates [16], phosphonates [17], as well as several polyalcohols [18]. Design and use of multifunctional ligands has been proven a particularly interesting approach to new structural motifs and often SMMs [19]. In the present work, the syntheses and properties are reported of several M/Gd (M = Mn and Fe) clusters incorporating a range of ligands, including simple carboxylates, tripodal alkoxides, and Schiff-based chelates (Scheme 1), all of which have been previously successful in bridging homometallic complexes. Furthermore, the possibility of obtaining Mn/Ln clusters with similar structural features as found in homonuclear complexes, despite the differences in the electronics and the relative sizes of 3d and 4f metals, provided additional motivation for this work.

2. Experimental

### 2.1. General and physical measurements

All manipulations were performed under aerobic conditions using materials (reagent grade) and solvents as received. $Mn(O_2CPh)_2 \cdot 2H_2O$ [20], $[Mn_3O(O_2CPh)_6(py)_2(H_2O)]$ [21], $[Mn_3O(O_2CBu^t)_6(py)_3]$ [21], and $[Fe_3O(O_2CBu^t)_6(H_2O)_3](OH)$ [22] were prepared as described.

Microanalyses (C, H, N) were performed by the in-house facilities of the Chemistry Department at the University of Florida. IR spectra (4000–450 cm^{-1}) were recorded on a Nicolet Nexus 670 spectrometer with samples prepared as KBr pellets. Variable-temperature dc and ac magnetic susceptibility data were collected at the University of Florida using a Quantum Design MPMS-XL SQUID susceptometer equipped with a 7 T magnet and operating in the 1.8–300 K range. Samples were embedded in solid eicosane to prevent torquing. Pascal's constants were used to estimate the diamagnetic corrections, which were subtracted from the experimental susceptibilities to give the molar paramagnetic susceptibilities (χ_M).

2.2. Compound preparation

2.2.1. $[Mn_2Gd_2O_2(O_2CBu^t)_8(HO_2CBu^t)_4]$ (**1**)

To a stirred solution of $Mn(O_2CMe)_2 \cdot 4H_2O$ (0.50 g, 2.0 mmol) in molten pivalic acid/water (40/15 mL) was added freshly prepared NBu_4MnO_4 (0.36 g, 1.0 mmol) and $Gd(O_2CMe)_3 \cdot xH_2O$ (0.83 g, 2.5 mmol). The solution was stirred overnight, filtered, and the filtrate layered with a mixture of acetone and ether. After 3 days, orange plate-like crystals had formed. The crystals were kept in mother liquor for the X-ray analysis, and dried under vacuum for other solid-state studies. Yield, 45%. *Anal.* Calc. for **1**·5H$_2$O: C, 44.85; H, 7.65; N, 0.00. Found: C, 44.51; H, 7.31; N, 0.02%. Selected IR data (KBr, cm^{-1}): 2977(bm), 2580(bw), 1702(vs), 1586(sm), 1485(vs), 1460(sm), 1415(sm), 1367(sm), 1304(vs), 1202(vs), 936(bm), 896(bm), 767(bm), 590(vs), 546(vs).
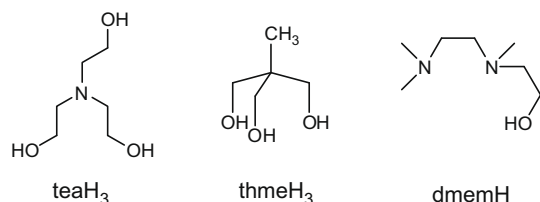
Scheme 1.

2.2.2. $[Mn_2Gd_2(OH)_2(O_2CPh)_4(NO_3)_2(teaH)_2]$ (**2**)

To a stirred solution of $[Mn_3O(O_2CPh)_6(py)_2(H_2O)]$ (0.27 g, 0.25 mmol) in MeCN (20 mL) was added teaH$_3$ (67 μL, 0.5 mmol) and solid $Gd(NO_3)_3 \cdot 6H_2O$ (0.45 g, 1.0 mmol). The reaction mixture was kept under magnetic stirring for 30 more minutes, and then filtered. The filtrate was left undisturbed for 2 days, during which time orange–brown plate-like crystals slowly formed. The crystals were maintained in the mother liquor for X-ray crystallography and other single-crystal studies, or collected by filtration, washed with Et$_2$O, and dried in vacuo. Yield, 80%. *Anal.* Calc. for **2**: C, 39.91; H, 4.02; N, 4.65. Found: C, 39.55; H, 3.72; N, 4.49%. Selected IR data (KBr, cm^{-1}): 3650(sm), 3241(bm), 2963(bm), 2883(bm), 1857(bm), 1597(vs), 1557(vs), 1438(s), 1383(vs), 1175(bw), 1081(vs), 904(s), 818(sw), 721(vs), 675(bm), 607(bm), 506(bm).

2.2.3. $[NHEt_3]_2[Fe_2Gd_2(O_2CPh)_4(thme)_2(NO_3)_4]$ (**3**)

An orange–red solution of $[Fe_3O(O_2CPh)_6(H_2O)_3](NO_3)$ (0.256 g, 0.25 mmol) in acetonitrile/methanol (10:1) was treated with $Gd(NO_3)_3 \cdot 6H_2O$ (0.34 g, 0.75 mmol), thmeH$_3$ (0.06 g, 0.5 mmol) and NEt$_3$ (0.14 mL, 1 mmol). The reaction mixture was kept under magnetic stirring for one hour, filtered, and the filtrate was left undisturbed for a period of 5 days, during which time orange–brown plate-like crystals slowly formed. The crystals of **3** were maintained in mother liquor for X-ray crystallography and other single-crystal studies, or collected by filtration, washed with Et$_2$O, and dried in vacuo. Yield, 25%. *Anal.* Calc. for **3**: C, 37.63; H, 4.60; N, 5.14. Found: C, 37.50; H, 4.66; N, 5.24%. Selected IR data (KBr, cm^{-1}): 2872(s), 2845(s), 2682(vs), 1599(m), 1559(m), 1488(mb), 1392(mb), 1298(m), 1176(sm), 1127(sm), 1056(m), 1022(m), 997(s), 836(s), 817(s), 727(m), 675(m), 609(sm), 581(sm), 454(bm), 411(vs).

2.2.4. $[Fe_2GdO(O_2CBu^t)_2(dmem)_2(NO_3)_3]$ (**4**)
2.2.4.1. Method A. To a stirred solution of dmemH (0.09 mL, 0.56 mmol) in EtOH (15 mL) was added solid $Gd(NO_3)_3 \cdot 6H_2O$ (0.19 g, 0.42 mmol) followed by $[Fe_3O(O_2CBu^t)_6(H_2O)_3](OH)$ (0.24 g, 0.28 mmol). The mixture was left under magnetic stirring for 2 h, and filtered to remove undissolved solid. Then Et$_2$O was allowed to diffuse into the filtrate, and X-ray quality crystals formed after 1 day. These were collected by filtration, washed with Et$_2$O, and dried in vacuo. Yield, 20%. *Anal.* Calc. for **4**: C, 29.91; H, 5.44; N, 10.17. Found: C, 29.89; H, 5.38; N, 10.09%. Selected IR data (cm^{-1}): 3425(m), 2975(m), 2907(m), 2841(m), 1563(s), 1487(s), 1424(s), 1380(s), 1302(s), 1228(m), 1179(w), 1113(w), 1086(s), 1061(m), 1029(m), 990(m), 936(w), 908(w), 888(m), 817(w), 787(m), 740(w), 688(m), 612(m), 581(m), 516(m), 443(m).

2.2.4.2. Method B. To a stirred solution of $Fe(NO_3)_3 \cdot 9H_2O$ (0.35 g, 0.87 mmol) and $Gd(NO_3)_3 \cdot 6H_2O$ (0.20 g, 0.44 mmol) in MeCN (15 mL) was added solid NaO_2CBu^t (0.06 g, 0.48 mmol), dmemH (0.14 mL, 0.86 mmol), and NEt$_3$ (0.12 mL, 0.86 mmol). The mixture was stirred for 2 h and filtered to remove undissolved solid. Then Et$_2$O was allowed to diffuse into the filtrate, and X-ray quality crystals formed after 2 days. The crystals were collected by filtration, washed with Et$_2$O, and dried in vacuo. Yield: 10%. The product was identified by IR spectral comparison and elemental analysis with material from Method A. *Anal.* Calc. for **4**: C, 29.91; H, 5.44; N, 10.17. Found: C, 30.21; H, 5.65; N, 9.81%.

2.2.5. $[Mn_2GdO(O_2CBu^t)_2(dmem)_2(NO_3)_3]$ (**5**)
2.2.5.1. Method A. To a stirred solution of $Mn(NO_3)_2 \cdot xH_2O$ (0.16 g, 0.89 mmol) and $Gd(NO_3)_3 \cdot 6H_2O$ (0.20 g, 0.44 mmol) in MeCN/ MeOH (12/1 mL) was added NaO_2CBu^t (0.06 g, 0.48 mmol), dmemH (0.14 mL, 0.86 mmol), and NEt$_3$ (0.18 mL, 1.28 mmol). The mixture was stirred for 3 h and filtered to remove undissolved solid. Then Et$_2$O was allowed to diffuse into the filtrate, and X-ray

quality crystals formed after 2 days. The crystals were collected by filtration, washed with Et$_2$O, and dried in vacuo. The yield was 20%. *Anal.* Calc. for **5**: C, 29.97; H, 5.45; N, 10.19. Found: C, 29.97; H, 5.45; N, 10.10%. Selected IR data (cm^{-1}): 3433(m), 2972(m), 2917(m), 2867(m), 2800(w), 1573(s), 1486(s), 1460(s), 1421(s), 1384(s), 1298(s), 1227(m), 1175(w), 1114(w), 1078(m), 1064(w), 1030(m), 1009(w), 990(w), 938(w), 907(w), 890(w), 818(w), 787(w), 740(w), 693(m), 645(w), 629(w), 586(w), 541(w), 517(w), 479(w).

2.2.5.2. Method B. To a stirred solution of dmemH (0.09 mL, 0.56 mmol) in MeCN/MeOH (13/2 mL) was added solid Gd(NO$_3$)$_3$·6H$_2$O (0.19 g, 0.42 mmol), and [Mn$_3$O(O$_2$CBu^t)$_6$(py)$_3$] (0.25 g, 0.24 mmol). The mixture was stirred for 2 h and filtered to remove undissolved solid. Reddish-orange needle-like crystals of **5** formed after two days upon vapor diffusion Et$_2$O into the filtrate. These were collected by filtration, washed with Et$_2$O, and dried in vacuo. Yield: 15%. The product was identified by IR spectral comparison and elemental analysis. *Anal.* Calc. for **5**: C, 29.97; H, 5.45; N, 10.19. Found: C, 29.99; H, 5.40; N, 10.01%.

2.3. Single-crystal X-ray crystallography

Data for all complexes were collected at 173 K on a Siemens SMART PLATFORM equipped with a CCD area detector and a graphite monochromator utilizing Mo Kα radiation (λ = 0.71073 Å). Suitable crystals of **1–5** were attached to glass fibers using silicone grease and transferred to a goniostat where they were cooled to 173 K for data collection. An initial search for reciprocal space revealed an orthorhombic cell for **1**, a triclinic for **2**, a monoclinic cell for **3**, and orthorhombic cells for **4** and **5**; the choices of space groups *Pbca* (**1**, **4**, **5**), $P\bar{1}$ (**2**), and $P2_1/n$ (**3**), were confirmed by the subsequent solution and refinement of the structures. Cell parameters were refined using up to 8192 reflections. A full sphere of data (1850 frames) was collected using the ω-scan method (0.3° frame width). The first 50 frames were re-measured at the end of data collection to monitor instrument and crystal stability (maximum correction on *I* was <1%). Absorption corrections by integration were applied based on measured indexed crystal faces. The structures were solved by direct methods in SHELXTL6 [23], and refined on F^2 using full-matrix least-squares. The non-H atoms were treated anisotropically, whereas the H atoms were placed in calculated, ideal positions and refined as riding on their respective C

atoms. Unit cell parameters and structure solution and refinement data are listed in Table 1.

For **1**, dimers of Mn$_2$Gd$_2$ are located on inversion centers. There is a disorder in the methyl groups on C27, which were refined in two parts with their site occupation factors dependently refined. Hydrogen atoms H1 and H3 on O atoms O1 and O3, respectively, were located from a difference Fourier map and refined without any constraints. A total of 427 parameters were refined in the final cycle of refinement using 7516 reflections with $I > 2\sigma(I)$ to yield R_1 and wR_2 of 2.98% and 6.69%, respectively. For **2**, the asymmetric unit consists of a half Mn$_2$Gd$_2$ cluster and three MeCN solvent molecules. Protons H1 and H7, on O1 and O7, respectively, were obtained from a Difference Fourier map and refined freely. A total of 405 parameters were refined in the final cycle of refinement using 6690 reflections with $I > 2\sigma(I)$ to yield R_1 and wR_2 of 2.62% and 6.13%, respectively. For **3**, the asymmetric unit consists of a half Fe$_2$Gd$_2$ cluster and one NHEt$_3^+$ cation; the H atom on the cation, H3, was located in a difference Fourier map and refined freely. A total of 392 parameters were refined in the final cycle of refinement using 6192 reflections with $I > 2\sigma(I)$ to yield R_1 and wR_2 of 2.76% and 6.33%, respectively. For **4**, the asymmetric unit consists of the Fe$_2$Gd cluster. A total of 451 parameters were refined in the final cycle of refinement using 5302 reflections with $I > 2\sigma(I)$ to yield R_1 and wR_2 of 3.60% and 6.66%, respectively. For **5**, the asymmetric unit consists of the Mn$_2$Gd cluster. The three methyl groups on C21 were disordered and were isotropically refined in three parts. A total of 463 parameters were refined in the final cycle of refinement using 7274 reflections with $I > 2\sigma(I)$ to yield R_1 and wR_2 of 2.58% and 6.43%, respectively.

3. Results and discussion

3.1. Syntheses

Several synthetic methods have been employed over the years to incorporate lanthanide ions into transition metal clusters. Probably the most successful one has been the reaction of a simple Mn^{II} salt with an oxidizing agent in the presence of a lanthanide source. Another approach is the reaction of a preformed transition metal cluster with a lanthanide salt. Both these methods have produced several mixed-metal carboxylate complexes [11a,11g,24]. However, the use of potentially chelating ligands combined with carboxylates has been poorly explored as a route to mixed-metal

Table 1
Crystallographic data for **1–5**.

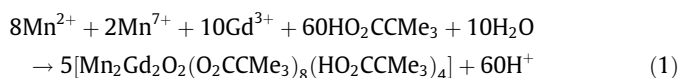| Parameter	1	2	3	4	5
Formula	C$_{60}$H$_{112}$Gd$_2$Mn$_2$O$_{26}$	C$_{52}$H$_{66}$Gd$_2$Mn$_2$N$_{10}$O$_{22}$	C$_{25}$H$_{35}$FeGdN$_3$O$_{13}$	C$_{24}$H$_{52}$Fe$_2$GdN$_7$O$_{16}$	C$_{24}$H$_{52}$Mn$_2$GdN$_7$O$_{16}$
Formula weight (g mol^{-1})	1673.88	1607.53	798.66	963.65	961.83
Space group	*Pbca*	$P\bar{1}$	$P2_1/n$	*Pbca*	*Pbca*
a (Å)	19.908(2)	12.064(1)	12.284(8)	18.4052(17)	18.2689(11)
b (Å)	18.578(2)	12.228(1)	17.046(11)	18.8604(18)	18.6402(11)
c (Å)	20.984(2)	12.879(1)	15.706(10)	22.168(2)	22.4775(14)
α (°)	90	117.284(1)	90	90	90
β (°)	90	94.928(1)	107.298(1)	90	90
γ (°)	90	102.558(1)	90	90	90
V (Å^3)	7761(1)	1610.0(2)	3139.9(4)	7695.3(13)	7654.4(8)
Z	4	1	4	8	8
T (°C)	−100(2)	−100(2)	−100(2)	−100(2)	−100(2)
Radiation (Å^a)	0.71073	0.71073	0.71073	0.71073	0.71073
ρ_{calc} (g cm^{-3})	1.433	1.658	1.689	1.664	1.669
μ (mm^{-1})	2.074	2.496	2.622	2.521	2.436
R_1 (wR_2) (%)^{b,c}	2.98(6.69)	2.38(6.13)	0.028(0.066)	0.036(0.067)	0.026(0.064)

^{a}Graphite monochromator.
^{b} $R_1 = \Sigma||F_o| - |F_c||/\Sigma|F_o|$.
^{c} $wR_2 = [\Sigma[w(F_o^2 - F_c^2)^2]/\Sigma[w(F_o^2)^2]]^{1/2}$ where S = $[\Sigma[w(F_o^2 - F_c^2)^2]/(n - p)]^{1/2}$, $w = 1/[\sigma^2(F_o^2) + (mp)^2 + np]$, $p = [\max(F_o^2, 0) + 2F_c^2]/3$, and m and n are constants.
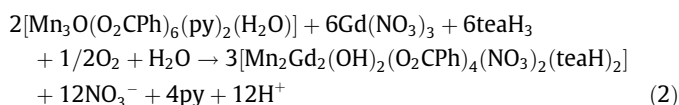
clusters. The complexes reported here were synthesized using a collection of these synthetic strategies.

Complex **1** was synthesized using pivalic acid as a co-solvent. Molten pivalic acid has been widely used in the synthesis of chromium clusters [25], but this is its first use in 3d–4f cluster chemistry to our knowledge. The comproportionation reaction we used resembles the synthesis of $[Mn_{12}O_{12}(O_2CMe)_{16}(H_2O)_4]$ [26] but in the presence of Gd^{3+} ions and using pivalic acid instead of acetic acid. Using $KMnO_4$ as an alternative source of Mn^{7+} ions produced the same product in a lower yield. The reaction of $Mn(O_2C-Me)_2 \cdot 4H_2O$, NBu_4MnO_4 and $Gd(O_2CMe)_3 \cdot xH_2O$ in a 2:1:2.5 molar ratio in a solvent mixture comprising of molten pivalic acid and water, gave a brown solution, which upon layering with ether/acetone led to the isolation of **1**. The stoichiometric reaction is summarized below in Eq. (1)

$$8Mn^{2+} + 2Mn^{7+} + 10Gd^{3+} + 60HO_2CCMe_3 + 10H_2O$$
$$\rightarrow 5[Mn_2Gd_2O_2(O_2CCMe_3)_8(HO_2CCMe_3)_4] + 60H^+ \qquad (1)$$

The use of excess of pivalic acid is critical in this synthesis, since the other solvent is water. The use of neat water as solvent in polynuclear $Mn^{III/IV}$ cluster chemistry would lead to hydrolysis and the formation of an insoluble MnO_x precipitate. However, under acidic conditions the latter is prevented, or at least minimized to a minor by-product, which can be separated by filtration. Analogues with other lanthanides can be obtained through the same procedure, which were identified by IR and elemental analysis, but they were not further characterized in this work.
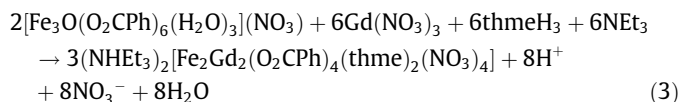
The reaction of a preformed triangular complex $[M_3O(O_2CR)_6L_3]^{0,+}$ (M = Fe, Mn, etc.; L = py, H_2O, etc.) complex with a chelating ligand represents a commonly employed and successful route to a wide range of higher nuclearity Mn clusters. For example, the use of triethanolamine ($teaH_3$) has led to a variety of products depending on the precise reaction conditions and ratios, including the largest iron cluster Fe_{64} [27l], Mn clusters with nuclearities currently up to 18, and a $Cu_{17}Mn_{28}$ cluster with T_d symmetry and $S = 51/2$ [27j], to highlight a few [27]. The alkoxide arms of the tea^{3-} ligand normally adopt bridging modes, fostering formation of higher nuclearity products. In the present work, the reaction of $[Mn_3O(O_2CPh)_6(py)_2(H_2O)]$, $Gd(NO_3)_3$ and $teaH_3$ in a 1:4:2 molar ratio in MeCN gave a brown solution from which orange–brown crystals of **2** slowly formed. The preparation of **2** can be summarized by Eq. (2)

$$2[Mn_3O(O_2CPh)_6(py)_2(H_2O)] + 6Gd(NO_3)_3 + 6teaH_3$$
$$+ 1/2O_2 + H_2O \rightarrow 3[Mn_2Gd_2(OH)_2(O_2CPh)_4(NO_3)_2(teaH)_2]$$
$$+ 12NO_3^- + 4py + 12H^+ \qquad (2)$$

The reactions are likely complicated equilibria involving several species of various nuclearities, both homo- and heterometallic, and the crystallization of the main product directly from the reaction solution is probably beneficial in providing pure material. The $teaH_3$ tripod has been used in the past in homonuclear Mn and Fe chemistry, producing several clusters with often high nuclearities and unusual metal topologies. In 3d/4f cluster chemistry, $teaH_3$ has afforded a small family of Fe_2Ln_2 (Ln = Ho, Dy, Tb) complexes [11e], which are structurally similar to **2** and **3** (*vide infra*).
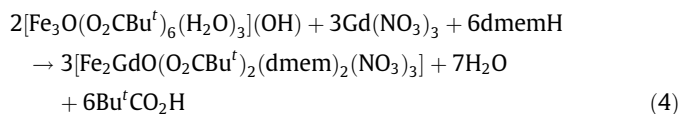
Tripodal $thmeH_3$ has been widely employed in the synthesis of various transition metal clusters with varying nuclearities, but its chemistry has proven significantly different from that of $teaH_3$ or other tripodal chelates [18b]. We thus decided to employ $thmeH_3$ in Fe/Ln reactions, using triangular iron clusters as starting materials; this methodology in homonuclear Fe cluster chemistry has in the past afforded a variety of products, including Fe_6 [28e,f], Fe_7 [28b], Fe_8 [28e], Fe_8 and Fe_{16} wheels [28a], Fe_{10} [14f,28d], and an Fe_{18} sigmoidal cluster [28c], to name a few [28]. In the present

work, the reaction of $[Fe_3O(O_2CPh)_6(H_2O)_3](NO_3)$ with $Gd(NO_3)_3 \cdot 6H_2O$ and $thmeH_3$ in the presence of NEt_3 in a 1:3:2:4 ratio in an acetonitrile/methanol (10:1) solvent mixture followed by slow evaporation led to the isolation of yellow crystals of **3** in 25% yield. The reaction is summarized in Eq. (3).
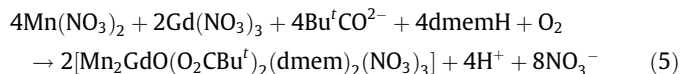
$$2[Fe_3O(O_2CPh)_6(H_2O)_3](NO_3) + 6Gd(NO_3)_3 + 6thmeH_3 + 6NEt_3$$
$$\rightarrow 3(NHEt_3)_2[Fe_2Gd_2(O_2CPh)_4(thme)_2(NO_3)_4] + 8H^+$$
$$+ 8NO_3^- + 8H_2O \qquad (3)$$

The same product can also be isolated from reactions with different reagent ratios, but in lower isolated yields.

The previous use of tridentate 2-{[2-(dimethylamino)ethyl]methylamino}ethanol (dmemH) in Fe chemistry has afforded several homometallic species [29]. As an extension to this work, dmemH was employed in both Fe/Ln and Mn/Ln reactions. Various reagent ratios and conditions were explored, and finally the reaction of $[Fe_3O(O_2CBu^t)_6(H_2O)_3](OH)$ with $Gd(NO_3)_3 \cdot 6H_2O$ and dmemH in a 2:3:4 ratio in EtOH followed by slow addition of Et_2O produced green crystals of $[Fe_2GdO(O_2CBu^t)_2(dmem)_2(NO_3)_3]$ (**4**) in 20–30% non-optimized yields (Method A of Experimental section). The reaction is summarized in Eq. (4).

$$2[Fe_3O(O_2CBu^t)_6(H_2O)_3](OH) + 3Gd(NO_3)_3 + 6dmemH$$
$$\rightarrow 3[Fe_2GdO(O_2CBu^t)_2(dmem)_2(NO_3)_3] + 7H_2O$$
$$+ 6Bu^tCO_2H \qquad (4)$$

The same product can be obtained from neat MeCN, but other products precipitate as well, which could not be separated and characterized. The same product was also obtained by treatment of an MeCN/MeOH solution of $Fe(NO_3)_3$ and $Gd(NO_3)_3$ with sodium pivalate and dmemH in a 2:1:1:2 ratio (Method B), but in a lower yield than that from Method A. Addition of extra base to the reaction did not change the identity of the product, but instead led to a small improvement in yield.

The reaction of $Mn(NO_3)_2 \cdot xH_2O$, $Gd(NO_3)_3 \cdot 6H_2O$, NaO_2CBu^t, dmemH, and NEt_3 in a 4:2:2:4:5 ratio in MeCN/MeOH produced a dark red solution, from which dark red crystals of $[Mn_2GdO(O_2C-Bu^t)_2(dmem)_2(NO_3)_3]$ (**5**) were obtained in 20% after addition of Et_2O. The reaction is summarized in Eq. (5)

$$4Mn(NO_3)_2 + 2Gd(NO_3)_3 + 4Bu^tCO_2^- + 4dmemH + O_2$$
$$\rightarrow 2[Mn_2GdO(O_2CBu^t)_2(dmem)_2(NO_3)_3] + 4H^+ + 8NO_3^- \qquad (5)$$

Attempts were made to increase the yield, and this could be achieved by small increases in the amounts of Gd^{3+} or $Bu^tCO_2^-$, but the product could only be obtained in a microcrystalline powder form under these conditions.

3.2. Description of structures

The complete structure and the partially labeled core of $[Mn_2Gd_2O_2(O_2CCMe_3)_8(HO_2CCMe_3)_4]$ (**1**) are shown in Fig. 1. Selected interatomic distances and angles are listed in Table 2. Compound **1** crystallizes in the orthorhombic space group *Pbca*. The compound contains a $[Mn_2^{III}Gd_2^{III}(\mu_3-O)_2]^{8+}$ core consisting of a Mn_2Gd_2 planar butterfly (or rhombus) with the Mn atoms at the body positions and each Mn_2Gd triangular unit bridged by a μ_3-O^{2-} ion (O13). The core is additionally mono-atomically bridged at each MnGd edge by an O atom of an $\eta^1:\eta^2:\mu$ pivalate group. The other four pivalates also bridge these edges, but in the more familiar $\eta^1:\eta^1:\mu$ triatomic modes, and the four pivalic acid groups are terminally bound to the two Gd atoms. The two Gd atoms are nine-coordinate with distorted capped square-antiprismatic geometry, and the two Mn atoms are six-coordinate with near-octahedral geometry. The Mn oxidation states were established by charge consider-
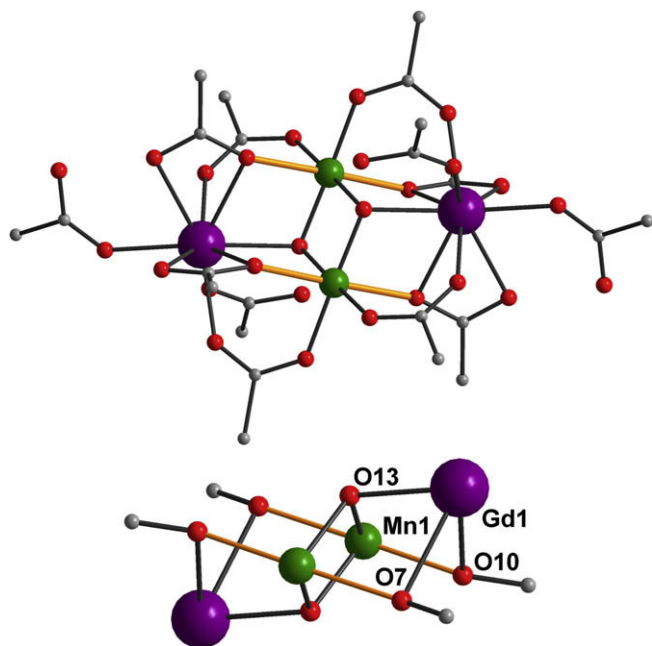
Fig. 1. The structure of complex **1** (top) and its partially labeled core (bottom). The Mn^{III} Jahn–Teller elongation axes are denoted as orange bonds. Color code: Mn^{III} green, Gd^{III} purple, O red, C gray. (For interpretation of the references in color in this figure legend, the reader is referred to the web version of this article.)

Table 2
Selected bond distances (Å) and angles (°) for complex **1**.

Gd1–O11	2.341(1)	Mn1–O5	1.960(2)
Gd1–O13	2.348 (1)	Mn1–O12′	1.967(2)
Gd1–O6	2.371 (1)	Mn1–O10′	2.188(2)
Gd1–O4	2.394(2)	Mn1–O7	2.266(2)
Gd1–O9	2.457(2)		
Gd1–O10	2.513(1)	Mn1–O7–Gd1	92.54(6)
Gd1–O7	2.518(2)	Mn1′–O10–Gd1	93.42(6)
Gd1–O2	2.523(2)	Mn1–O13–Mn1′	98.24(8)
Gd1–O8	2.527(2)	Mn1–O13–Gd1	108.84(8)
Gd1–O11	2.341(2)	Mn1′–O13–Gd1	107.16(8)
Gd1–O13	2.348(2)		
Mn1–O13	1.895(2)	Gd1···Mn1′	3.429(1)
Mn1–O13′	1.901(2)	Mn1···Mn1′	2.870(1)

Symmetry code: ′ = −x, −y + 2, −z.

ations, bond-valence sum calculations (Table 3), and their clear Jahn–Teller (JT) axial elongations; as expected, the elongated Mn^{III}–O bonds are 0.1–0.2 Å longer than the other Mn^{III}–O bonds. In addition, these JT axes are in a normal orientation, containing carboxylate O atoms and thus avoiding the short Mn–O^{2-} bonds. As a result, the JT axes are parallel and are oriented roughly along the long axis of the core. All terminal pivalic acids form intramolecular

Table 3
Bond valence sum calculations and assignments for the Mn[a] ions in complexes **1**, **2**, and **5**.

Complex	Mn ion	Mn^{II}	Mn^{III}	Mn^{IV}
1	Mn1	2.97	<u>2.73</u>	2.84
2	Mn1	3.00	<u>2.77</u>	2.87
5	Mn1	3.12	<u>2.90</u>	2.97
	Mn2	3.16	<u>2.93</u>	3.00

[a] The underlined value is the one closest to the charge for which it was calculated. The oxidation state can be taken as the whole number nearest to the bond value.

hydrogen-bonds to adjacent oxygen atoms (average O···O distance 2.567 Å). There are no intermolecular hydrogen-bonds. Finally, it should be noted that a similar compound to **1** has been previously obtained from a different synthetic procedure involving the reaction of a preformed Mn$_6$ pivalate cluster with Gd(NO$_3$)$_3$ in a CH$_2$Cl$_2$/MeOH mixture. This previous compound differs from **1** in possessing terminal MeOH groups on the Gd atoms, rather than pivalic acids [24a].

The complete structure and the partially labeled core of [Mn$_2$Gd$_2$(OH)$_2$(O$_2$CPh)$_4$(NO$_3$)$_2$(teaH)$_2$] (**2**) are shown in Fig. 2. Selected interatomic distances and angles are listed in Table 4. Complex **2** crystallizes in triclinic space group $P\bar{1}$ with the cluster lying on an inversion center. The structure is overall similar to that of **1**, but with some distinct differences: it consists of a Mn$_2^{III}$Gd$_2^{III}$ planar butterfly (rhombus) with each Mn$_2$Gd triangle bridged by a μ$_3$-OH$^-$ ion (oxygen atoms O1 and O1′); the Mn oxidation states and the protonated nature of the μ$_3$-OH$^-$ ions were confirmed by BVS calculations on the Mn (Table 3) and the O atoms (Table 5). Each of the two teaH^{2-} groups is a tetradentate chelate to a Gd atom, with the protonated alcohol arms (O7) binding terminally to the Gd, and the two deprotonated alkoxide arms (O6, O8) each bridging to an adjacent Mn atom. There is also a chelating NO$_3^-$ group on each Gd atom, and ligation is completed by an η^1:η^1:μ-O$_2$CPh$^-$ group bridging each MnGd edge of the rhombus. The Mn and Gd atoms are six- and nine-coordinate, respectively. The Mn atoms are again JT axially elongated, but, unlike the situation in **1**, they now lie roughly along the short axis of the rhombus and contain the μ$_3$-OH$^-$ ions. Intermolecular hydrogen-bonds are present in **2**; one of the nitrate oxygen atoms (O11) is hydrogen-bonded to protonated
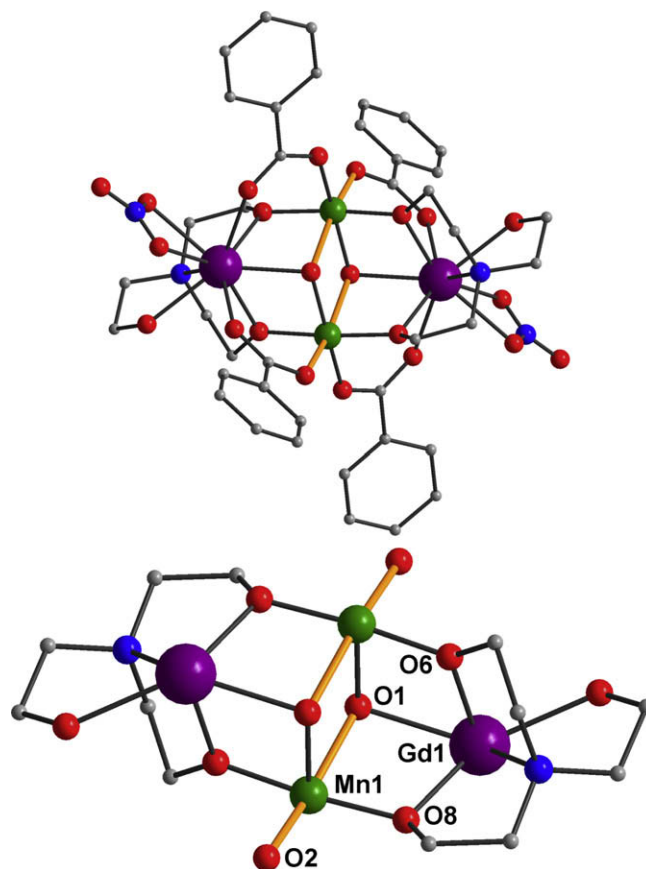
Fig. 2. The structure of complex **2** (top) and its partially labeled core (bottom). The Mn^{III} Jahn–Teller elongation axes are denoted as orange bonds. Color code: Mn^{III} green, Gd^{III} purple, O red, N blue, C gray. (For interpretation of the references in color in this figure legend, the reader is referred to the web version of this article.)

Table 4
Selected bond distances (Å) and angles (°) for complex **2**.

Gd1–O6	2.329(1)	Mn1–O5	1.953(2)
Gd1–O3	2.331(1)	Mn1–O1	1.973(2)
Gd1–O1	2.370(1)	Mn1–O2	2.176(2)
Gd1–O8	2.397(1)	Mn1–O1′	2.209(2)
Gd1–O4′	2.428(1)		
Gd1–O7	2.444(1)	Mn1–O1–Mn1′	103.69(7)
Gd1–O10	2.535(1)	Mn1–O1–Gd1	101.74(7)
Gd1–O9	2.541(1)	Mn1′–O1–Gd1	97.71(7)
Gd1–N1	2.614(2)		
Mn1–O6	1.885(1)	Gd1···Mn1	3.3784(4)
Mn1–O8′	1.899(1)	Gd1···Mn1′	3.4503(4)

Symmetry code: ′ = −x + 1, −y + 1, −z + 1.

Table 5
Bond valence sum calculations and assignments for the triply-bridging O[a] ions in complexes **1**, **2**, **4**, and **5**.

Complex	O atom	BVS	Assignment
1	O13	1.79	O^{2-}
2	O1	1.31	OH^{-}
4	O1	2.02	O^{2-}
5	O1	2.02	O^{2-}

[a] An O BVS in the ~1.8–2.0, ~1.0–1.2 and ~0.2–0.4 ranges is indicative of non-, single- and double-protonation, respectively.

arm (O7) of the $teaH^{2-}$ ligand, thus creating a one-dimensional hydrogen-bonded array of Mn_2Gd_2 complexes (see Supplementary data).

The overall structures of the cores of complexes **1** and **2** can also be described as two face-sharing $[M_4O_4]$ cubanes with a metal atom missing from one vertex of each cubane. Such a "defective dicubane" unit with a resulting planar M_4 rhombus is relatively common in both homo- and heterometallic cluster chemistry [11f,24a,30], and is often on a crystallographic center of symmetry. The biggest difference between the two cores is the identity of the μ_3-O atoms, being O^{2-} versus OH^{-} in **1** and **2**, respectively. This then leads to the other major difference between **1** and **2**, the positions of the Mn^{III} JT axes, which lie along the Mn^{III}-μ_3-OH^{-} bonds in **2**. This is reasonable given the longer nature of Mn^{III}-μ_3-OH^{-} bonds compared with Mn^{III}-μ_3-O^{2-} ones, and this is also the situation commonly seen in Mn_4 "defective dicubanes" where the μ_3-O atoms are alkoxides.

The complete structure and the partially labeled core of the $[Fe_2Gd_2(O_2CPh)_4(thme)_2(NO_3)_4]^{2-}$ anion of **3** are shown in Fig. 3. Selected interatomic distances and angles are listed in Table 6. Complex **3** crystallizes in the monoclinic space group $P2_1/n$ with the cluster lying on an inversion center. The core consists of a planar Fe_2Gd_2 rhombus and a "defective dicubane" topology as in **1** and **2**, but now all μ_2 and μ_3 monoatomic bridges are the alkoxide arms of two $thme^{3-}$ groups, each bound in the $\eta^2{:}\eta^2{:}\eta^3{:}\mu_4$ bridging mode. Each FeGd edge of the rhombus is additionally bridged by an $\eta^1{:}\eta^1{:}\mu$-O_2CPh^{-} group. There are also two chelating (η^2) nitrate ions on each Gd atom. Both Fe ions are six-coordinate with distorted octahedral geometries, while the Gd atoms are both nine-coordinate with distorted capped square-antiprismatic geometries. Note that although **2** and **3** both contain tripod-like chelate groups, there are some very important differences: (i) the ligand $thme^{3-}$ in **3** is bound in a very different way than the $teaH^{2-}$ in **2**; (ii) the μ_3–O atoms are alkoxides from the $thme^{3-}$ arms in **3**, whereas they are μ_3-OH^{-} ions in **2**; and (iii) the ligation of the Gd ions in **3** is completed by two chelating NO_3^{-} ions, whereas by only one in **2**. These are no doubt also significantly responsible for the differences in the M···Gd distances (3.45(4) and 3.38(4) Å
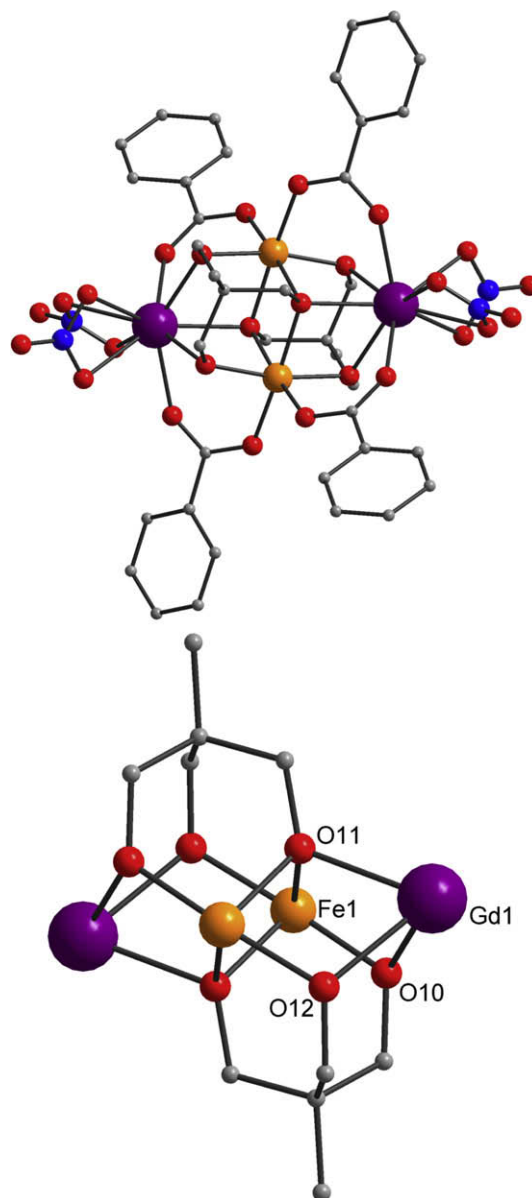
Fig. 3. The structure of complex **3** (top) and its partially labeled core (bottom). Color code: Fe^{III} orange, Gd^{III} purple, O red, N blue, C gray. (For interpretation of the references in color in this figure legend, the reader is referred to the web version of this article.)

Table 6
Selected bond distances (Å) and angles (°) for complex **3**.

Fe1–O10′	1.9563(17)	Gd1–O10′	2.3621(17)
Fe1–O12	1.9649(17)	Gd1–O2	2.3641(19)
Fe1–O1	1.9994(19)	Gd1–O12′	2.3719(18)
Fe1–O13	2.0034(17)	Gd1–O3	2.3908(17)
Fe1–O11′	2.0901(18)	Gd1–O11	2.4066(17)
Fe1–O11	2.1072(17)	Gd1–O8	2.4778(18)
Gd1–O4	2.633(2)	Gd1–O7	2.481(2)
Gd1–N2	2.895(2)	Gd1–O5	2.5472(19)
Gd1–O12–Fe1	104.78(2)	Gd1–O11–Fe1′	99.17(2)
Fe1–O10–Gd1′	105.31(2)	Fe1–O10–Fe1′	99.14(4)

for Mn···Gd in **2** versus 3.44(4) Å for both Fe···Gd in **3**), the M···M distances (3.29(5) Å for the Mn···Mn in **2** versus 3.19(3) Å for Fe···Fe in **3**), and the M-μ_3-O-Gd angles (97.71(7)° and 101.74(7)° in **2** versus 99.8(2)° and 104.8(2)° in **3**). Thus, the two

complexes are significantly different, even though their cores appear to be similar.
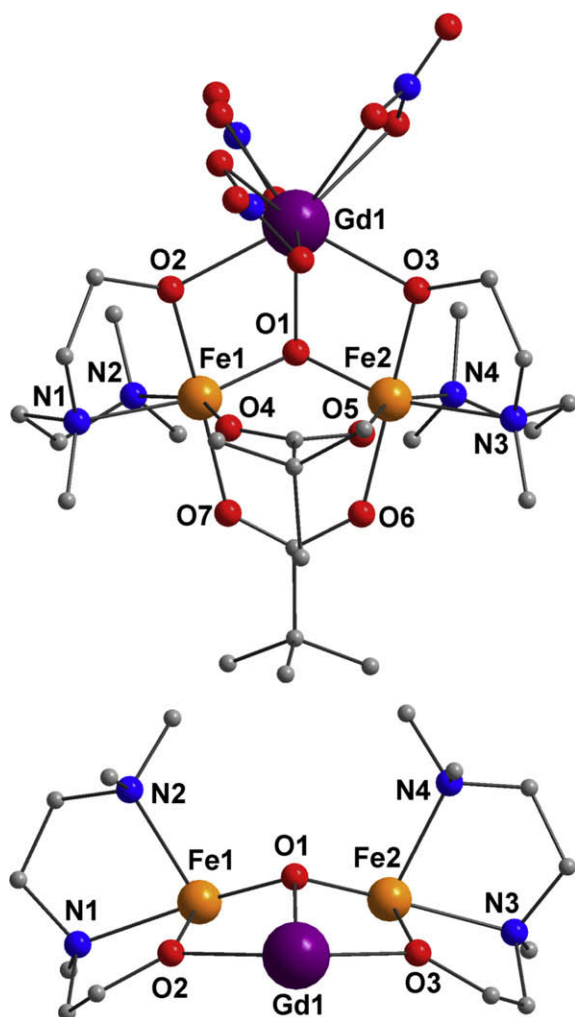
The complete structure and the labeled core of [Fe$_2$GdO(O$_2$C-Bu^t)$_2$(dmem)$_2$(NO$_3$)$_3$] (**4**) are shown in Fig. 4. Selected interatomic distances and angles are listed in Table 7. Complex **4** crystallizes in the orthorhombic space group *Pbca*. The structure consists of two Fe^{III} ions and one Gd^{III} atom in a triangular arrangement bridged by a central μ$_3$-O^{2-} ion (O1). The triangular unit is essentially isosceles (Fe1···Fe2 = 3.172(8) Å, Fe1/Fe2···Gd1 = 3.362(7) Å) with the oxide 0.645 Å out of the Fe$_2$Gd plane. The Fe1···Fe2 edge is bridged by two η^1:η^1:μ-O$_2$CBu$^t-$ groups while the Fe1/Fe2···Gd1 edge is bridged by an alkoxide O atom of the dmem$^-$ ligand. Three chelating (η^2) nitrates complete the ligation of each nine-coordinate Gd ion, while the Fe atoms are six-coordinate with distorted octahedral geometries.

The complete structure and the partially labeled core of [Mn$_2$GdO(O$_2$CBu^t)$_2$(dmem)$_2$(NO$_3$)$_3$] (**5**) are shown in Fig. 5. Selected interatomic distances and angles are listed in Table 8. Complex **5** crystallizes in the orthorhombic space group *Pbca*. Complex **5** is essentially isostructural with **4**, the only difference being the Mn atoms in place of Fe. The Mn^{III} oxidation state was established by charge balance considerations and inspection of Mn–O and Mn–N bond distances, and confirmed quantitatively by bond-va-

lence sum (BVS) calculations (Table 3). The Mn^{III} centers are both six-coordinate with distorted octahedral geometries, and exhibit a JT axial elongation along the O4–Mn1–N4 and O5–Mn2–N2 axes, each involving a carboxylate O and dmem N atom. It should be added that such triangular oxide-centered M$_2$Ln complexes (**4** and **5**) are unprecedented in the literature; only the recently re-

Table 7
Selected bond distances (Å) and angles (°) for complex **4**.

Fe1–O1	1.848(3)	Fe2–N4	2.232(3)
Fe1–O2	1.959(3)	Gd1–O3	2.321(3)
Fe1–O7	2.030(3)	Gd1–O2	2.367(3)
Fe1–O4	2.061(3)	Gd1–O1	2.368(3)
Fe1–N1	2.216(4)	Gd1–O12	2.462(3)
Fe1–N2	2.242(3)	Gd1–O9	2.473(3)
Fe2–O1	1.841(3)	Gd1–O8	2.479(3)
Fe2–O3	1.978(3)	Gd1–O11	2.502(3)
Fe2–O6	2.031(3)	Gd1–O15	2.505(3)
Fe2–O5	2.040(3)	Gd1–O14	2.544(3)
Fe2–N3	2.197(4)		
Fe2–O1–Fe1	118.60(14)	Fe1–O2–Gd1	101.56(12)
Fe2–O1–Gd1	105.34(11)	Fe2–O3–Gd1	102.57(11)
Fe1–O1–Gd1	105.10(12)		

Fig. 4. The structure of complex **4** (top) and its partially labeled core (bottom). Color code: Fe^{III} orange, Gd^{III} purple, O red, N blue, C gray. (For interpretation of the references in color in this figure legend, the reader is referred to the web version of this article.)
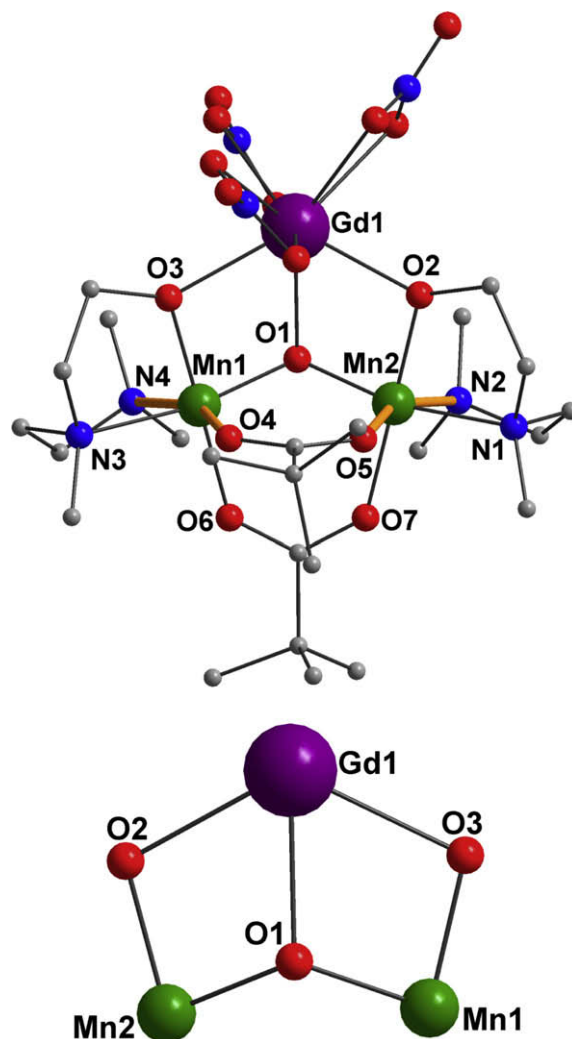
Fig. 5. The structure of complex **5** (top) and its partially labeled core (bottom). The Mn^{III} Jahn–Teller elongation axes are denoted as orange bonds. Color code: Mn^{III} green, Gd^{III} purple, O red, N blue, C gray. (For interpretation of the references in color in this figure legend, the reader is referred to the web version of this article.)

Table 8
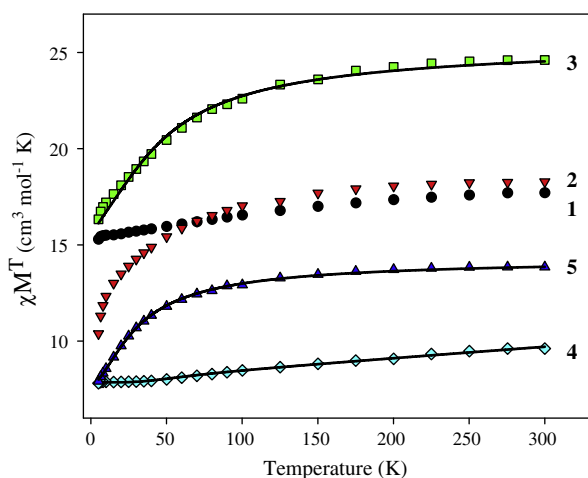Selected bond distances (Å) and angles (°) for complex **5**.

Mn1–O1	1.8398 (15)	Mn2–N2	2.352(2)
Mn1–O3	1.9042(16)	Gd1–O2	2.3350(16)
Mn1–O6	1.9703(17)	Gd1–O2	2.3471(15)
Mn1–N3	2.114(2)	Gd1–O3	2.3754(16)
Mn1–O4	2.2868(18)	Gd1–O11	2.4759(19)
Mn1–N4	2.379(2)	Gd1–O15	2.479(2)
Mn2–O1	1.8373(15)	Gd1–O12	2.4813(19)
Mn2–O2	1.9162(16)	Gd1–O14	2.4894(19)
Mn2–O7	1.9855(17)	Gd1–O9	2.506(2)
Mn2–N1	2.096(2)	Gd1–O8	2.527(2)
Mn2–O5	2.1531(18)		
Mn2–O1–Mn1	120.47(8)	Mn2–O2–Gd1	102.67(7)
Mn2–O1–Gd1	104.79(7)	Mn1–O3–Gd1	102.34(7)
Mn1–O1–Gd1	105.50(7)		

ported [MnGd$_2$O(O$_2$CPh)$_3$(O$_2$CMe)(dapdo)(dapdoH)$_2$] (dapdoH$_2$ = 2,6-diacetylpyridine dioxime) is currently known [12b], but this is different from **4** and **5** in having an excess of the Ln atoms over the 3d metal.

3.3. Magnetochemistry

3.3.1. Dc magnetic susceptibility studies

Solid state, variable-temperature magnetic susceptibility measurements were performed on vacuum-dried microcrystalline samples of complexes **1–5** suspended in eicosane to prevent torquing. The dc molar magnetic susceptibility (χ_M) data were collected in the 5.0–300 K range in a 0.1 T (1000 Oe) magnetic field, and are shown in Fig. 6 as $\chi_M T$ versus T plots. For complex **1**, $\chi_M T$ is ~17.7 cm^3 K mol^{-1} at 300 K, gradually decreasing with decreasing temperature to ~15.6 cm^3 K mol^{-1} at 25.0 K, below which it is essentially constant until a small final drop to ~15.3 cm^3 K mol^{-1} at 5.0 K. The $\chi_M T$ value at 300 K is lower than the spin-only value ($g = 2$) of ~21.8 cm^3 K mol^{-1} expected for two Mn^{III} ($S = 2$) and two Gd^{III} ($S = 7/2$) non-interacting ions, which indicates antiferromagnetic interactions between the metal centers. For **2**, $\chi_M T$ is ~18.3 cm^3 K mol^{-1} at 300 K, remains essentially constant down to 150 K, and then decreases gradually with decreasing temperature to ~10.4 cm^3 K mol^{-1} at 5.0 K. The 300 K value and the overall profile are again indicative of dominant antiferromagnetic interactions between the metal centers. For **3**, $\chi_M T$ is ~24.5 cm^3 K mol^{-1} at 300 K, which is the expected value for four non-interacting me-

tal ions (2 Fe^{III}, 2 Gd^{III}), and then gradually decreases with decreasing temperature to ~16.3 cm^3 K mol^{-1} at 5 K.

The isotropic Heisenberg–Dirac–VanVleck (HDVV) spin Hamiltonian describing the exchange interactions within the butterfly (rhombus) M$_4$ topology of **1–3** with effective C_{2v} symmetry is given by Eq. (6), where J_1 denotes the Mn$\cdots$Mn interaction between the 'body' Mn atoms, and J_2 denotes the Mn$\cdots$Gd interactions on the four edges. $\hat{S}_i$ ($i = 1$–4) is the spin

$$\mathcal{H} = -2J_1\hat{S}_1 \cdot \hat{S}_3 - 2J_2(\hat{S}_1 \cdot \hat{S}_2 + \hat{S}_1 \cdot \hat{S}_4 + \hat{S}_2 \cdot \hat{S}_3 + \hat{S}_3 \cdot \hat{S}_4) \quad (6)$$

operator for metal atom M$_i$ ($i = 1$ and 3 for M; $i = 2$ and 4 for Gd). The Gd$\cdots$Gd exchange interaction (J_3) is assumed to be zero and is omitted from Eq. (6). The eigenvalues of Eq. (6) can be determined analytically using the Kambe vector coupling method [31] and the substitutions $\hat{S}_A = \hat{S}_1 + \hat{S}_3$, $\hat{S}_B = \hat{S}_2 + \hat{S}_4$, and $\hat{S}_T = \hat{S}_A + \hat{S}_B$ ($\hat{S}_T$ is the total spin of the molecule), as described previously [32]. The resulting eigenvalue expression is given in Eq. (7), where E$|S_T, S_A, S_B>$ is the energy of state S_T arising from spin vectors S_A and S_B, and

$$E|S_T, S_A, S_B> = -J_1[S_A(S_A + 1)] - J_2[S_T(S_T + 1) - S_T(S_T + 1) - S_B(S_B + 1)] \quad (7)$$

constant terms contributing to all terms have been omitted. Thus, an expression for the molar paramagnetic susceptibility, χ_M, can be derived using the above and the Van Vleck equation [33], and assuming an isotropic g tensor. This equation can then be used to fit the experimental $\chi_M T$ versus T data in Fig. 6 as a function of the two exchange parameters J_1 and J_2, and the g factor. For complex **1**, we could not get an acceptable fit, which we assume is due to all interactions being very weak, which is as expected for 3d–4f and even commonly Mn$^{III}\cdots$Mn^{III} interactions [11e–g,12b,24a,34]. In accordance with this, a similar problem was encountered for **2**. Different variations of the temperature-independent paramagnetism (TIP) and the paramagnetic impurity terms also failed to provide us with a reasonable fit for the data. For **3**, the problem was not so severe, presumably due to the stronger nature of Fe$^{III}_2$ interactions. In fact, a satisfactory fit was obtained for **3** assuming the magnitude of the Fe–Gd coupling to be negligible compared to the Fe$\cdots$Fe coupling, i.e. $J_2 \sim 0$. Fitting of the data revealed an antiferromagnetic Fe$\cdots$Fe interactions, with $J = -3.4(1)$ cm^{-1} and $g = 2.07(5)$.
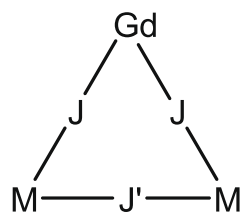
For trinuclear complex **4**, $\chi_M T$ decreases from 9.60 cm^3 K mol^{-1} at 300 K to 7.81 cm^3 K mol^{-1} at 5.0 K. The 300 K value is much lower than the spin-only ($g = 2$) value of 16.63 cm^3 K mol^{-1} expected for two non-interacting Fe^{III} and one Gd^{III} spins, suggesting strong antiferromagnetic interactions within this molecule. The 5 K value suggests an $S = 7/2$ ground state. For **5**, $\chi_M T$ steadily decreases from 13.60 cm^3 K mol^{-1} at 300 K to 7.91 cm^3 K mol^{-1} at 5.0 K. The 300 K value is only slightly less than the spin-only ($g = 2$) value of 13.87 cm^3 K mol^{-1} expected for two non-interacting Mn^{III} and one Gd^{III} spin centers, suggesting weaker antiferromagnetic interactions in **5** than in **4**, as expected for the Mn^{III} versus Fe^{III} difference. Again, the $\chi_M T$ value at 5 K suggests an $S = 7/2$ ground state for **5**.

The pairwise Fe$\cdots$Fe and Fe$\cdots$Gd exchange interactions in **4** were obtained by fitting the variable-temperature susceptibility data to the appropriate theoretical expression. An isosceles triangle model was used involving two exchange parameters, and the resulting isotropic Heisenberg spin Hamiltonian is given by Eq. (8), where $\hat{S}_1$, $\hat{S}_2$, and $\hat{S}_3$ are the spins of Fe1, Fe2, and

$$\mathcal{H} = -2J(\hat{S}_1 \cdot \hat{S}_2 + \hat{S}_3 \cdot \hat{S}_2) - 2J'\hat{S}_1 \cdot \hat{S}_3 \quad (8)$$

Gd1, respectively, and J and J' are the Fe^{III}Gd^{III} and Fe^{III}Fe^{III} exchange interactions (Scheme 2).

The eigenvalues of Eq. (8) can again be determined using the Kambe vector coupling method, with the substitutions $\hat{S}_A = \hat{S}_1 + \hat{S}_3$

Fig. 6. $\chi_M T$ versus T plots for complexes **1–5** in the temperature range 5.0–300 K in 0.1 T applied dc field. The solid lines, where available, are fits to the experimental data; see the text for the fit parameters.

Scheme 2.

and $\hat{S}_T = \hat{S}_A + \hat{S}_2$, and these are given in Eq. (9), where constant terms contributing to all terms have been omitted.

$$E|S_T, S_A >= -J[S_T(S_T + 1) - S_A(S_A + 1)] - J'[S_A(S_A + 1)] \quad (9)$$

For complex **4**, $S_1 = S_2 = 5/2$; $S_3 = 7/2$ and the overall multiplicity of the spin system is 288, made up of 32 individual spin states ranging from $S_T = 1/2$ to $17/2$. An expression for the molar para-magnetic susceptibility was derived for this complex using the Van Vleck equation. This was then used to fit the experimental $\chi_M T$ versus T data, with fit parameters of J, J' and an isotropic g value. The fit is shown as the solid line in Fig. 6, which gave $J' = -59(3)$ cm^{-1}, $J = 1.2(3)$ cm^{-1}, and $g = 2$. This indicates the ground state to be the $|S_T, S_A> = |7/2, 0>$, i.e. the Fe^{III} spins are aligned perfectly antiparallel ($S_A = 0$); owing to the large difference in magnitude between J and $|J'|$ ($J/J' = 0.02$), the J magnetic pathway is completely frustrated in its preference to align the two Fe spins antiparallel to the Gd spin and thus parallel to each other.

To confirm the above ground state conclusion for **4**, magnetization (M) data were collected in the 0.1–7 T and 1.8–10 K ranges. The resulting data are shown in Fig. 7 (top) as a reduced magnetization ($M/N\mu_B$) versus H/T plot, where N is Avogadro's number and μ_B is the Bohr magneton. The saturation value at the highest fields and lowest temperatures is $\sim$7.0, as expected for an $S = 7/2$ spin state and with g slightly less than 2; the saturation value should be gS in the absence of complications from low-lying excited states or significant anisotropy. The data were fit, using the program MAG-NET [35], by diagonalization of the spin Hamiltonian matrix assuming only the ground state is populated, incorporating axial anisotropy ($D\hat{S}_z^2$) and the Zeeman interaction, and employing a full powder average. The corresponding spin Hamiltonian is given by Eq. (10), where $\hat{S}_z$ is the z-axis spin operator, μ_0 is the vacuum permeability, and H is

$$H = D\hat{S}_z^2 + g\mu_B\mu_0\hat{S}\cdot H \quad (10)$$

the applied field. The last term in Eq. (10) is the Zeeman term associated with the applied magnetic field. The best fit for **4** is shown as the solid lines in Fig. 7 (top), and gave fit parameters of $S = 7/2$ and either of two sets of parameters: $g = 2.01$ and $D = 0.15$ cm^{-1}, or $g = 2.01$ and $D = -0.14$ cm^{-1}. It is common to obtain two acceptable fits of magnetization data for a given S value, one with $D > 0$ and the other with $D < 0$, since magnetization fits are not very sensitive to the sign of D. In order to assess which is the superior fit for **4**, and also to ensure that the true global minimum had been located, the root-mean-square error surface was calculated for the fit as a function of D and g using the program GRID [36], which calculates the relative difference between the experimental $M/N\mu_B$ data and those calculated for various combinations of D and g. For **4**, the error surface clearly shows the two minima with positive and negative D values, with both fits being of comparable quality (see Supplementary data). It is thus not possible to safely conclude from these magnetization fits what the true sign of D is, and more sensitive techniques such as EPR is required.

Magnetization data were collected similarly for complex **5**, but a satisfactory fit of the resulting $M/N\mu_B$ versus H/T plots could not be obtained using all the data collected up to 7 T. This is typically
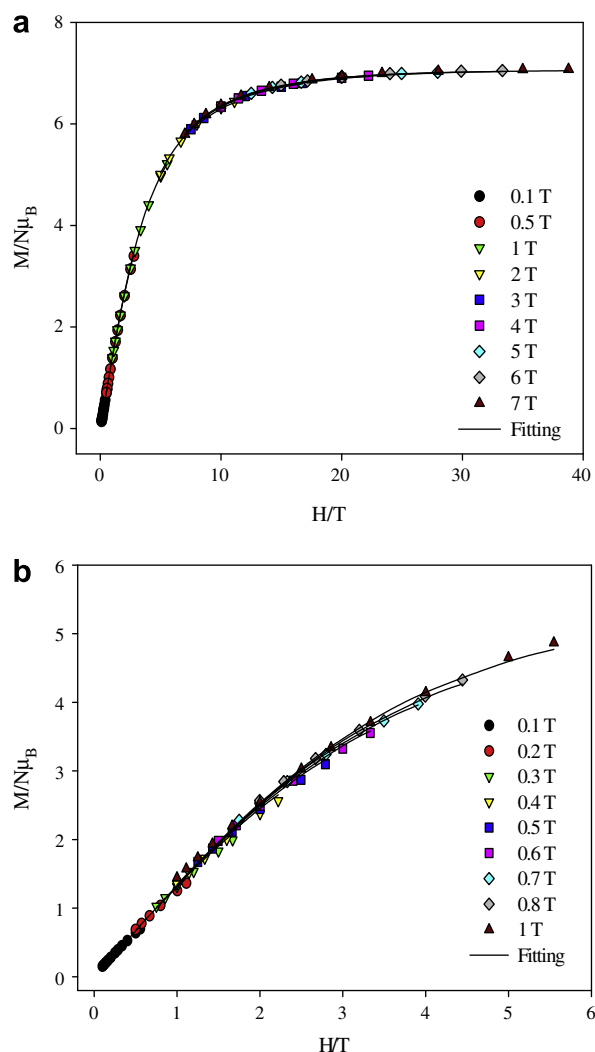

Fig. 7. Plots of the reduced magnetization, $M/N\mu_B$ versus H/T (a) for complex **4** in the field range 0.1–7 T; (b) for complex **5** in the field range 0.1–1 T. The solid lines are fits with negative D; see the text for the fit parameters.

the case when low-lying excited states are present, and we have found that such complications can often be avoided if only lower field data are considered [15a,e,29,37]. Indeed, a satisfactory fit (solid lines in Fig. 7 (bottom)) was obtained for **5** using data for fields only up to 1.0 T, with fit parameters $S = 7/2$, $D = -0.16$ cm^{-1}, and $g = 1.9$. This is again in agreement with the preliminary estimate from the data in Fig. 6. Similar problems assignable to low-lying excited states were also encountered in attempts to fit reduced magnetization data for complexes **1–3**, but in these cases not even the use of only low-field data would allow acceptable fits to be achieved. We thus resorted to AC susceptibility studies.

3.3.2. Ac magnetic susceptibility studies

In order to determine or confirm the ground state spins of complexes **1–5**, alternating current (AC) magnetic susceptibility measurements were performed in the 1.8–15 K temperature range in a 3.5 Oe AC field oscillating at 50–1000 Hz. The in-phase (χ_M') components of the AC magnetic susceptibilities for **1–5** are presented in Fig. 8 as $\chi_M'T$ versus T plots. The in-phase signal for **1** is essentially constant in this temperature range at $\sim$16 cm^3 K mol^{-1}, which is as expected for two uncoupled $S = 7/2$ Gd^{III} atoms (15.8 cm^3 K mol^{-1} for $g = 2$), suggesting the Mn^{III} spins have paired by this temperature leaving only the Gd^{III} spins uncoupled. There is
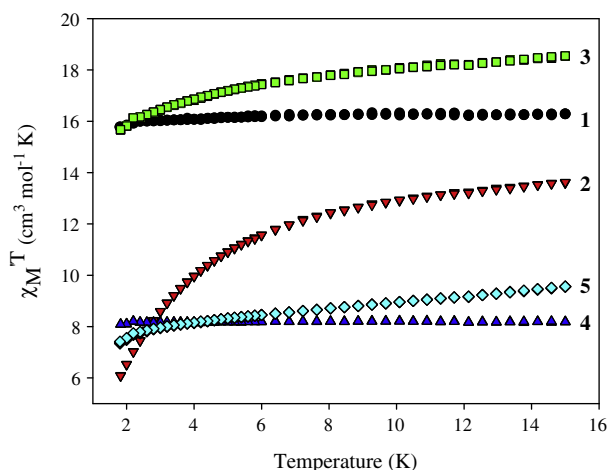
Fig. 8. Plot of the in-phase (χ_M') ac magnetic susceptibility as $\chi_M'T$ versus T in a 3.5 Oe field oscillating at the frequency range 50–1000 Hz for complexes **1–5**.

no out-of-phase (χ_M'') signal for **1**, i.e., as expected this complex is not a SMM.

In contrast to **1**, the (χ_M')T for complex **2** decreases only slightly with temperature down to ~7 K and then more steeply to ~6 cm^3 K mol^{-1} at 1.8 K, and seems to be heading to ~0 at 0 K. Since intermolecular hydrogen-bonding was observed in the structure of **2** (vide supra), we assign the steep drop below 7 K to weak intermolecular antiferromagnetic interactions, whose effect will only become evident at the lowest temperatures. Extrapolation to 0 K of the data above ~7 K gives a value of ~10 cm^3 K mol^{-1}, suggesting an $S \sim 4$ ground state but with likely many low-lying excited states. Such an intermediate ground state is also consistent with spin frustration effects, as expected in triangular units with competing exchange interactions. This would suggest that, unlike the case in **1**, the Mn···Gd coupling is stronger in **2** than in **1**, which is consistent with the differing orientations of the JT axes in the two complexes, and thus the d$_{z^2}$ magnetic orbital which lies along it. Again, no χ_M'' signal was observed for this complex.

For complex **3**, the $\chi_M'T$ decreases only slightly with decreasing temperature from ~18.5 cm^3 K mol^{-1} at 15 K to ~15.7 cm^3 K mol^{-1} at 1.8 K. This suggests a situation analogous to that in **1**, i.e. the Fe^{III} spins are antiparallel aligned as a result of their antiferromagnetic interaction, leaving the two Gd spins uncoupled as a result of very weak Gd···Fe interactions.

For complex **4**, $\chi_M'T$ is essentially constant at ~8 cm^3 K mol^{-1}, which is analogous to the proposed situation in **3**, i.e. that the Fe spins are paired and the observed $\chi_M'T$ is due to an $S = 7/2$ ground state arising from the uncoupled Gd spin (7.9 cm^3 K mol^{-1} for $g = 2$). For complex **5**, the overall $\chi_M'T$ profile is similar to **4**, and an analogous rationalization is proposed that therefore assumes that the Mn···Mn coupling is stronger than the Gd···Mn one.

4. Summary and conclusions

A series of new transition metal–lanthanide species have been obtained from the use of a variety of synthetic methods employing carboxylates and a range of chelating ligands, except in the case of complex **1** for which no chelate was employed and which therefore is a purely carboxylato-bridged Mn$_2$Gd$_2$ cluster. Complex **2** is analogous to **1**, but contains a tripodal chelating ligand, teaH^{2-}. Complex **2** is also Mn$_2$Gd$_2$ and has no exact precedent in the inorganic literature, but is similar to some Fe$_2$Ln$_2$ complexes previously reported. From the use of the tripodal thmeH$_3$ chelate in Fe–Gd chemistry, a related Fe$_2$Gd$_2$ complex was obtained. In contrast to these M$_2$Ln$_2$ complexes **1–3**, the use of dmemH has provided

two oxide-centered trinuclear M–Gd clusters with M = Fe (**4**) or Mn (**5**), which are both unprecedented in the literature. It is clear that the employment of various chelates in mixed 3d/4f cluster chemistry offers the continuing possibility of new and interesting types of mixed-metal clusters, and work in this area is continuing.

Appendix A. Supplementary data

CCDC 729493, 729494, 729492, 729491, and 729490 contain the supplementary crystallographic data for **1–5**. These data can be obtained free of charge via http://www.ccdc.cam.ac.uk/conts/retrieving.html, or from the Cambridge Crystallographic Data Centre, 12 Union Road, Cambridge CB2 1EZ, UK; fax: (+44) 1223 336 033; or e-mail: deposit@ccdc.cam.ac.uk. Supplementary data associated with this article can be found, in the online version, at doi:10.1016/j.poly.2009.06.003.

References

[1] (a) B. Sieve, X. Chen, J. Cowen, P. Larson, S.D. Mahanti, M.G. Kanatzidis, Chem. Mater. 11 (1999) 2451;
(b) S.E. Latturner, D. Bilc, S.D. Mahanti, M.G. Kanatzidis, Chem. Mater. 14 (2002) 1695;
(c) M.A. Zhuravleva, J. Salvador, D. Bilc, S.D. Mahanti, J. Ireland, C.R. Kannewurf, M.G. Kanatzidis, Chem. Eur. J. 10 (2004) 3197;
(d) M.G. Kanatzidis, R. Pöttgen, W. Jeitschko, Angew. Chem., Int. Ed. Engl. 44 (2005) 2;
(e) X. Wu, Intermetallics 14 (2006) 114;
(f) H.-U. Habermeier, Mater. Today 10 (2007) 34.
[2] (a) T. Kimura, Annu. Rev. Mater. Res. 37 (2007) 387;
(b) S.-W. Cheong, M. Mostovoy, Nat. Mater. 6 (2007) 13;
(c) R. Ramesh, N.A. Spaldin, Nat. Mater. 6 (2007) 21;
(d) C.-L. Jia, V. Nagarajan, J.-Q. He, L. Houben, T. Zhao, R. Ramesh, K. Urban, R. Waseret, Nat. Mater. 6 (2007) 64;
(e) P. Muralt, Nat. Mater. 6 (2007) 8;
(f) H. Schmid, Ferroelectrics 162 (1994) 317;
(g) T. Goto, H. Shintani, K. Ishizaka, T. Arima, Y. Tokura, T. Kimura, Nature 426 (2003) 55;
(h) S. Park, P.A. Sharma, J.S. Ahn, S. Guha, S-W. Cheong, N. Hur, Nature 429 (2004) 392;
(i) N. Ikeda, H. Ohsumi, K. Ohwada, K. Ishii, T. Inami, K. Kakurai, Nature 436 (2005) 1136.
[3] (a) D. Coucouvanis, Acc. Chem. Res. 24 (1991) 1;
(b) B.K. Burgess, D.J. Lowe, Chem. Rev. 96 (1996) 2983.
[4] D.T. Sawyer, J.S. Valentine, Acc. Chem. Res. 14 (1981) 392.
[5] (a) N. Strater, P. Klabunde, R. Tucker, H. Witzel, B. Krebs, Science 268 (1995) 1489;
(b) M.B. Twitchette, A.G. Sykes, Eur. J. Inorg. Chem. 12 (1999) 2105.
[6] (a) A. Guskov, J. Kern, A. Gabdulkhakov, M. Broser, A. Zouni, W. Saenger, Nat. Struct. Mol. Biol. 16 (2009) 334;
(b) J. Barber, J.W. Murray, Phil. Trans. R. Soc. B. 363 (2008) 1129;
(c) K.N. Ferreira, T.M. Iverson, K. Maghlaoui, J. Barber, S. Iwata, Science 303 (2004) 1831;
(d) J. Barber, Inorg. Chem. 47 (2008) 1700;
(e) J. Yano, J. Kern, K. Sauer, M.J. Latimer, Y. Pushkar, J. Biesiadka, B. Loll, W. Saenger, J. Messinger, A. Zouni, V.K. Yachandra, Science 314 (2006) 821;
(f) K. Sauer, J. Yano, V.K. Yachandra, Photosynth. Res. 85 (2005) 73.
[7] (a) J.C. Fontecilla-Camps, A. Volbeda, C. Cavazza, Y. Nicolet, Chem. Rev. 107 (2007) 4273;
(b) A. Volbeda, J.C. Fontecilla-Camps, Coord. Chem. Rev. 249 (2005) 1609.
[8] (a) M. Andruh, J.P. Costes, C. Diaz, S. Gao, Inorg. Chem. 48 (2009) 3342;
(b) C. Benelli, D. Gatteschi, Chem. Rev. 102 (2002) 2369;
(c) R.E.P. Winpenny, Chem. Soc. Rev. 27 (1998) 447;
(d) F. Mori, T. Nyui, T. Ishida, T. Nogami, K.Y. Choi, H. Nojiri, J. Am. Chem. Soc. 125 (2003) 8694;
(e) N. Ishikawa, Polyhedron 26 (2007) 2147.
[9] (a) G. Christou, Polyhedron 24 (2005) 2065;
(b) R. Sessoli, D. Gatteschi, D.N. Hendrickson, G. Christou, MRS Bull. 25 (2000) 66;
(c) R. Sessoli, D. Gatteschi, A. Caneschi, M.A. Novak, Nature 365 (1993) 141.
[10] (a) R. Bagai, G. Christou, Chem. Soc. Rev. 38 (2009) 1011;
(b) R. Sessoli, H.-L. Tsai, A.R. Schake, S. Wang, J.B. Vincent, K. Folting, D. Gatteschi, G. Christou, D.N. Hendrickson, J. Am. Chem. Soc. 115 (1993) 1804.

[11] (a) T.C. Stamatatos, S.J. Teat, W. Wernsdorfer, G. Christou, Angew. Chem., Int. Ed. Engl. 48 (2009) 521;
(b) A.M. Ako, V. Mereacre, R. Clérac, W. Wernsdorfer, I.J. Hewitt, C.E. Anson, A.K. Powell, Chem. Commun. (2009) 544;
(c) V. Mereacre, A.M. Ako, R. Clerac, W. Wernsdorfer, I.J. Hewitt, C.E. Anson, A.K. Powell, Chem. Eur. J. 14 (2008) 3577;
(d) V. Mereacre, A.M. Ako, R. Clerac, W. Wernsdorfer, G. Filoti, J. Bartolome, C.E. Anson, A.K. Powell, J. Am. Chem. Soc. 129 (2007) 9248;
(e) M. Murugesu, A. Mishra, W. Wernsdorfer, K.A. Abboud, G. Christou, Polyhedron 25 (2006) 613;
(f) A. Mishra, W. Wernsdorfer, S. Parsons, G. Christou, E.K. Brechin, Chem. Commun. (2005) 2086;
(g) A. Mishra, W. Wernsdorfer, K.A. Abboud, G. Christou, J. Am. Chem. Soc. 126 (2004) 15648;
(h) S. Osa, T. Kido, N. Matsumoto, N. Re, A. Pochaba, J. Mrozinski, J. Am. Chem. Soc. 126 (2004) 420;
(i) C.M. Zaleski, E.C. Depperman, J.W. Kampf, M.L. Kirk, V.L. Pecoraro, Angew. Chem., Int. Ed. Engl. 43 (2004) 3912;
(j) A.J. Tasiopoulos, W. Wernsdorfer, B. Moulton, M.J. Zaworotko, G. Christou, J. Am. Chem. Soc. 125 (2003) 15274.
[12] (a) C. Benelli, A.J. Blake, P.E.Y. Milne, J.M. Rawson, R.E.P. Winpenny, Chem. Eur. J. 1 (1996) 614;
(b) C. Lampropoulos, T.C. Stamatatos, K.A. Abboud, G. Christou, Inorg. Chem. 48 (2009) 429;
(c) C. Benneli, D. Gatteschi, Chem. Rev. 102 (2002) 2369.
[13] O. Kahn, Molecular Magnetism, VCH Publishers, New York, 1993.
[14] (a) H.J. Eppley, H.L. Tsai, N. Devries, K. Folting, G. Christou, D.N. Hendrickson, J. Am. Chem. Soc. 117 (1995) 301;
(b) N.E. Chakov, M. Soler, W. Wernsdorfer, K.A. Abboud, G. Christou, Inorg. Chem. 44 (2005) 5304;
(c) A. Cornia, A.C. Fabretti, P. Pacchioni, L. Zobbi, D. Bonacchi, A. Caneschi, D. Gatteschi, R. Biagi, U.D. Pennino, V.D. Renzi, L. Gurevich, H.S.J. Van der Zant, Angew. Chem., Int. Ed. Engl. 42 (2003) 1645;
(d) P. Artus, C. Boskovic, J. Yoo, W.E. Streib, L.-C. Brunel, D.N. Hendrickson, G. Christou, Inorg. Chem. 40 (2001) 4199;
(e) M. Soler, P. Artus, K. Folting, J.C. Huffman, D.N. Hendrickson, G. Christou, Inorg. Chem. 40 (2001) 4902;
(f) R. Bagai, G. Christou, Inorg. Chem. 46 (2007) 10810;
(g) T.C. Stamatatos, A.G. Christou, S. Mukherjee, K.M. Poole, C. Lampropoulos, K.A. Abboud, T.A. O'Brien, G. Christou, Inorg. Chem. 47 (2008) 9021;
(h) C. Lampropoulos, T.C. Stamatatos, K.A. Abboud, G. Christou, Polyhedron 28 (2009) 1958.
(i) J.J. Henderson, C.M. Ramsey, E. del Barco, A. Mishra, G. Christou, J. Appl. Phys. 101 (2007) 09E102.
[15] (a) C. Lampropoulos, C. Koo, S.O. Hill, K.A. Abboud, G. Christou, Inorg. Chem. 47 (2008) 11180;
(b) R.C. Squire, S.M.J. Aubin, K. Folting, W.E. Streib, G. Christou, D.N. Hendrickson, Inorg. Chem. 34 (1995) 6463;
(c) C. Canada-Vilalta, W.E. Streib, J.C. Huffman, T.A. O'Brien, R.E. Davidson, G. Christou, Inorg. Chem. 43 (2004) 101;
(d) M.W. Wemple, H.L. Tsai, S. Wang, J.P. Claude, W.E. Streib, J.C. Huffman, D.N. Hendrickson, G. Christou, Inorg. Chem. 35 (1996) 6437;
(e) C. Lampropoulos, M. Murugesu, K.A. Abboud, G. Christou, Polyhedron 26 (2007) 2129;
(f) M. Pacchioni, A. Cornia, A.C. Fabretti, L. Zobbi, D. Bonacchi, A. Caneschi, G. Chastanet, D. Gatteschi, R. Sessoli, Chem. Commun. (2004) 2604.
[16] (a) C.J. Milios, E. Kefalloniti, C.P. Raptopoulou, A. Terzis, R. Vicente, N. Lalioti, A. Escuer, S.P. Perlepes, Chem. Commun. (2003) 819;
(b) C. Dendrinou-Samara, M. Alexiou, C.M. Zaleski, J.W. Kampf, M.L. Kirk, D.P. Kessissoglou, V.L. Pecoraro, Angew. Chem., Int. Ed. Engl. 42 (2003) 3763;
(c) C.M. Zaleski, E.C. Depperman, C. Dendrinou-Samara, M. Alexiou, J.W. Kampf, D.P. Kessissoglou, M.L. Kirk, V.L. Pecoraro, J. Am. Chem. Soc. 127 (2005) 12862;
(d) T.C. Stamatatos, V. Nastopoulos, A.J. Tasiopoulos, E.E. Moushi, W. Wernsdorfer, G. Christou, S.P. Perlepes, Inorg. Chem. 47 (2008) 10081;
(e) C.C. Stoumpos, I.A. Gass, C.J. Milios, N. Lalioti, A. Terzis, G. Aromi, S.J. Teat, E.K. Brechin, S.P. Perlepes, Dalton Trans. (2009) 307;
(f) T.C. Stamatatos, K.A. Abboud, W. Wernsdorfer, G. Christou, Angew. Chem., Int. Ed. Engl. 47 (2008) 6694;
(g) G.S. Papaefstathiou, S.P. Perlepes, Comments Inorg. Chem. (2002) 249;
(h) P. Chaudhuri, Coord. Chem. Rev. 243 (2003) 143;
(i) C.J. Milios, T.C. Stamatatos, S.P. Perlepes, Polyhedron 25 (2006) 134;
(j) C.J. Milios, R. Inglis, A. Vinslava, A. Prescimone, S. Parsons, S.P. Perlepes, G.Christou,E.K. Brechin, Chem. Commun. (2007) 2738.
[17] (a) E.I. Tolis, M. Helliwell, S. Langley, J. Raftery, R.E.P. Winpenny, Angew. Chem., Int. Ed. Engl. 42 (2003) 3804;
(b) M. Shanmugam, G. Chastanet, T. Mallah, R. Sessoli, S.J. Teat, G.A. Timco, R.E.P. Winpenny, Chem. Eur. Jour. 12 (2006) 8777.
[18] (a) A.J. Tasiopoulos, S.P. Perlepes, Dalton Trans. (2008) 5537;
(b) T.C. Stamatatos, K.A. Abboud, W. Wernsdorfer, G. Christou, Angew. Chem., Int. Ed. Engl. 46 (2007) 884;
(c) E.K. Brechin, Chem. Commun. (2005) 5141;
(d) C. Lampropoulos, K.A. Abboud, T.C. Stamatatos, G. Christou, Inorg. Chem. 48 (2009) 813;
(e) A.M. Ako, I.J. Hewitt, V. Mereacre, R. Clérac, W. Wernsdorfer, C.E. Anson, A.K. Powell, Angew. Chem., Int. Ed. Engl. 45 (2006) 4926;

[19] (a) T.C. Stamatatos, K.A. Abboud, G. Christou, Dalton Trans. (2009) 41;
(b) T. Taguchi, T.C. Stamatatos, K.A. Abboud, C.M. Jones, K.M. Poole, T.A. O'Brien, G. Christou, Inorg. Chem. 47 (2008) 4095;
(c) R. Bagai, K.A. Abboud, G. Christou, Inorg. Chem. 47 (2008) 621;
(d) R. Bagai, W. Wernsdorfer, K.A. Abboud, G. Christou, J. Am. Chem. Soc. 129 (2007) 12918.
[20] M.W. Wemple, H.-L. Tsai, S. Wang, J.P. Claude, W.E. Streib, J.C. Huffman, D.N. Hendrickson, G. Christou, Inorg. Chem. 35 (1996) 6437.
[21] J.B. Vincent, H.R. Chang, K. Folting, J.C. Huffman, G. Christou, D.N. Hendrickson, J. Am. Chem. Soc. 109 (1987) 5703.
[22] (a) J.F. Duncan, C.R. Kanekar, K.F. Mok, J. Chem. Soc. A 3 (1969) 480;
(b) A. Earnshaw, B.N. Figgis, J. Lewis, J. Chem. Soc. A 12 (1966) 1656;
(c) R.W. Wu, M. Poyraz, F.E. Sowrey, C.E. Anson, S. Wocadlo, A.K. Powell, U.A. Jayasooriya, R.D. Cannon, T. Nakamoto, M. Katada, H. Sano, Inorg. Chem. 37 (1998) 1913.
[23] SHELXTL6, Bruker-AXS, Madison, WI, 2000.
[24] (a) C. Benelli, M. Murrie, S. Parsons, R.E.P. Winpenny, J. Chem. Soc., Dalton Trans. (1999) 4125;
(b) C. Turta, D. Prodius, V. Mereacre, S. Shova, M. Gdaniec, Y.A. Simonov, V. Kuncser, G. Filoti, A. Caneschi, L. Sorace, Inorg. Chem. Commun. 7 (2004) 576;
(c) X.-M. Chen, M.-L. Tong, Y.-L. Wu, Y.-J. Luo, J. Chem. Soc., Dalton Trans. (1996) 2181;
(d) Q.-D. Liu, S. Gao, J.-R. Li, Q.-Z. Zhou, K.-B. Yu, B.-Q. Ma, S.-W. Zhang, X.-X. Zhang, T.-Z. Jin, Inorg. Chem. 39 (2000) 2488;
(e) J.-J. Zhang, T.-L. Sheng, S.-Q. Xia, G. Leibeling, F. Meyer, S.-M. Hu, R.-B. Fu, S.-C. Xiang, X.-T. Wu, Inorg. Chem. 43 (2004) 5472.
[25] (a) G.A. Timco, E.J.L. McInnes, R.G. Pritchard, F. Tuna, R.E.P. Winpenny, Angew. Chem., Int. Ed. Engl. 47 (2008) 9681;
(b) M. Rancan, G.N. Newton, C.A. Muryn, R.G. Pritchard, G.A. Timco, L. Cronin, R.E.P. Winpenny, Chem. Commun. (2008) 1560;
(c) E.J.L. McInnes, S. Piligkos, G.A. Timco, R.E.P. Winpenny, Coord. Chem. Rev. 249 (2005) 2577;
(d) C.-F. Lee, D.A. Leigh, R.G. Pritchard, D. Schultz, S.J. Teat, G.A. Timco, R.E.P. Winpenny, Nature 458 (2009) 314.
[26] T. Lis, Acta Crystallogr. B36 (1980) 2042.
[27] (a) M. Murugesu, K.A. Abboud, G. Christou, Dalton Trans. (2003) 4552;
(b) I. Krabbes, W. Seichter, K. Gloe, Acta Crystallogr., Sect. C. 56 (2000) 178;
(c) Y. Chen, Q. Liu, Y. Deng, H. Zhu, C. Chen, H. Fan, D. Liao, E. Gao, Inorg. Chem. 40 (2001) 3725;
(d) O. Waldmann, R. Koch, S. Schromm, J. Schu1lein, P. Mu1ller, I. Bernt, R.W. Saalfrank, F. Hampel, E. Balthes, Inorg. Chem. 40 (2001) 2986;
(e) M. Murugesu, W. Wernsdorfer, K.A. Abboud, G. Christou, Angew. Chem., Int. Ed. Engl. 44 (2005) 892;
(f) B. Pilawa, M.T. Kelemen, S. Wanka, A. Geisselmann, A.L. Barra, Europhys. Lett. 43 (1998) 7;
(g) M.I. Khan, S. Tabussum, R.J. Doedens, V.O. Golub, C.J. O'Connor, Inorg. Chem. 43 (2004) 5850;
(h) L.F. Jones, P. Jensen, B. Moubaraki, K.J. Berry, J.F. Boas, J.R. Pilbrow, K.S. Murray, J. Mater. Chem. 16 (2007) 435;
(i) S. Shah, C.M. Ramsey, K.J. Heroux, J.R. O'Brien, A.G. Dipasquale, A.L. Rheingold, E. del Barco, D.N. Hendrickson, Inorg. Chem. 47 (2008) 6245;
(j) A. Zhou, W. Zhang, M. Tong, X. Chen, M. Nakano, C.C. Beedle, D.N. Hendrickson, J. Am. Chem. Soc. 129 (2007) 1014;
(k) G. Rajaraman, M. Murugesu, E.C. Sanudo, M. Soler, W. Wernsdorfer, M. Helliwell, C. Muryn, J. Raftery, S.J. Teat, G. Christou, E.K. Brechin, J. Am. Chem. Soc. 126 (2004) 15445;
(l) T. Liu, Y.-J. Zhang, Z.-M. Wang, S. Gao, J. Am. Chem. Soc. 130 (2008) 10500.
[28] (a) L.F. Jones, A. Batsanov, E.K. Brechin, D. Collison, M. Helliwell, T. Mallah, E.J.L. McInnes, S. Piligkos, Angew. Chem., Int. Ed. Engl. 41 (2002) 4318;
(b) R. Bagai, K.A. Abboud, G. Christou, Chem. Commun. (2007) 3359;
(c) S. Parsons, G.A. Solan, R.E.P. Winpenny, C. Benelli, Angew. Chem., Int. Ed. Engl. 35 (1996) 1825;
(d) E.K. Brechin, M.J. Knapp, J.C. Huffman, D.N. Hendrickson, G. Christou, Inorg. Chim. Acta 297 (2000) 389;
(e) C.A. Christmas, H.L. Tsai, L. Pardi, J.M. Kesselman, P.K. Gantzel, R.K. Chadha, D. Gatteschi, D.F. Harvey, D.N. Hendrickson, J. Am. Chem. Soc. 115 (1993) 12483;
(f) M. Murugesu, K.A. Abboud, G. Christou, Polyhedron 23 (2004) 2779;
(g) K.L. Taft, S.J. Lippard, J. Am. Chem. Soc. 112 (1990) 9629.
[29] R. Bagai, S. Datta, A. Betancur-Rodriguez, K.A. Abboud, S. Hill, G. Christou, Inorg. Chem. 46 (2007) 4535.
[30] O. Roubeau, R. Clérac, Eur. J. Inorg. Chem. (2008) 4325. and references therein.
[31] K. Kambe, J. Phys. Soc. Jpn. 5 (1950) 48.
[32] (a) J.B. Vincent, C. Christmas, H.R. Chang, Q. Li, P.D.W. Boyd, J.C. Huffman, D.N. Hendrickson, G. Christou, J. Am. Chem. Soc. 111 (1989) 2086;
(b) E. Libby, J.K. McCusker, E.A. Schmitt, K. Folting, D.N. Hendrickson, G. Christou, Inorg. Chem. 30 (1991) 3486;
(c) G. Aromí, S. Bhaduri, P. Artús, J.C. Huffman, D.N. Hendrickson, G. Christou, Polyhedron 21 (2002) 1779;

(d) S. Wang, K. Folting, W.E. Streib, E.A. Schmitt, J.K. McCusker, D.N. Hendrickson, G. Christou, Angew. Chem., Int. Ed. Engl. 30 (1991) 305;
(e) G. Aromí, S. Bhaduri, P. Artús, K. Folting, G. Christou, Inorg. Chem. 41 (2002) 805;
(f) C. Cañada- Vilalta, J.C. Huffman, G. Christou, Polyhedron 20 (2001) 1785;
(g) J.K. McCusker, J.B. Vincent, E.A. Schmitt, M.L. Mino, K. Shin, D.K. Coggin, P.M. Hagen, J.C. Huffman, G. Christou, D.N. Hendrickson, J. Am. Chem. Soc. 113 (1991) 3012.
[33] J.H. Van Vleck, The Theory of Electric and Magnetic Susceptibilities, Oxford Press, London, 1932.

[34] A. Panagiotopoulos, T.F. Zafiropoulos, S.P. Perlepes, E. Bakalbassis, I. Masson-Ramade, O. Kahn, A. Terzis, C.P. Raptopoulou, Inorg. Chem. 34 (1995) 4918.
[35] E. R. Davidson, Magnet, Indiana University, Bloomington, IN, 1999.
[36] E.R. Davidson, GRID, Indiana University, Bloomington, IN, 1999.
[37] (a) M. Soler, W. Wernsdorfer, K. Folting, M. Pink, G. Christou, J. Am. Chem. Soc. 126 (2004) 2156;
(b) E.C. Sanudo, W. Wernsdorfer, K.A. Abboud, G. Christou, Inorg. Chem. 43 (2004) 4137;
(c) M. Murugesu, J. Raftery, W. Wernsdorfer, G. Christou, E.K. Brechin, Inorg. Chem. 43 (2004) 4203.